Spectrochimica Acta Part A: Molecular and Biomolecular Spectroscopy 326 (2025) 125206

Contents lists available at ScienceDirect

Spectrochimica Acta Part A: Molecular and Biomolecular Spectroscopy

journal homepage: www.journals.elsevier.com/spectrochimica-acta-part-a-molecular-and-biomolecular-spectroscopy

Could Raman spectroscopy investigate the changes of cell oxidative stress status in thyroid diseases? A pilot study on cytological samples

Michael Di Gioacchino [a,*], Martina Verri [a,b], Anda Mihaela Naciu [c], Alessio Paolucci [a], Alessandra di Masi [a], Chiara Taffon [b], Andrea Palermo [c], Anna Crescenzi [b,d], Maria Antonietta Ricci [a], Armida Sodo [a]

[a] Dipartimento di Scienze, Università degli studi Roma Tre, Roma, Italy
[b] Pathology of Endocrine Organs and Neuromuscolar Pathology Unit, Fondazione Policlinico Universitario Campus Bio-Medico, Roma, Italy
[c] Unit of Metabolic Bone and Thyroid Disorders, Fondazione Policlinico Universitario Campus Bio-Medico, Roma, Italy
[d] Department of Oncological Radiological and Pathological Sciences, Università degli studi La Sapienza of Rome, Roma, Italy

HIGHLIGHTS

- Raman spectroscopy has been applied to cytological thyroid samples.
- Cells redox status is assessed by oxidated/reduced cytochromes bands intensity ratio.
- Raman analysis is sensible to changes of oxidative stress during the time.
- Carotenoids uptake is likely used as antioxidant scavenger against oxidative stress.

GRAPHICAL ABSTRACT

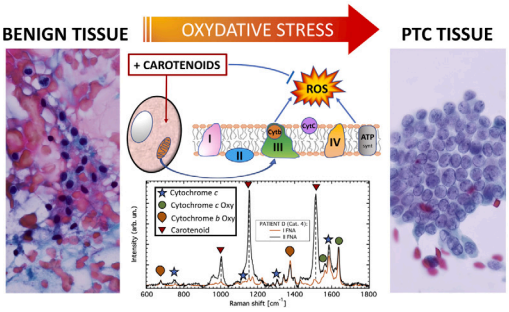

ARTICLE INFO

Keywords:
Thyroid cancer
Oxidative stress
Raman spectroscopy
Caroternoids
Cytochrome *c*
Cytochrome *b*

ABSTRACT

The incidence of thyroid nodules is rapidly increasing worldwide. Raman spectroscopy (RS) is a powerful label-free and non-invasive technique, successfully used for early stage diagnosis. Here, RS is proposed as a tool to investigate the thyroid disease, including neoplasms, through the study of cell oxidative stress (OS), which represents one of the main cancer risk factors. In this study, we enrolled 28 patients, submitted to a first and second thyroid fine needle aspiration (FNA) during follow up. The cytological samples were studied by RS and morphological examination. Typical Raman spectra of thyroid cytological samples are reported and the contribution of oxidized and reduced cytochrome *b* and *c* and carotenoids are discussed. On the basis of the evolution of the Raman features over the time lapse between the two FNAs, the 28 patients have been classified into 4 different categories and the most representative case for each category is reported and discussed in detail. For each category, the different Raman intensity ratio between oxidized and reduced cytochromes *b* and *c* is reported and associated to different cell OS status, along with the presence of carotenoids. Overall, our results support a correlation among changes in oxidative stress, carotenoids uptake and thyroid diseases, which could inspire new fundamental research on biomarkers and signaling pathways involved in thyroid OS.

* Corresponding author.
E-mail address: michael.digioacchino@uniroma3.it (M. Di Gioacchino).

https://doi.org/10.1016/j.saa.2024.125206
Received 15 April 2024; Received in revised form 18 September 2024; Accepted 22 September 2024
Available online 26 September 2024

1. Introduction

Thyroid is an endocrine gland that plays a fundamental role in the metabolic regulations through hormones production and secretion. In basal conditions, this induces a physiological production of reactive oxygen species (ROS) in thyrocytes [1,2]. Therefore, the internal enzymatic defense system (e.g. superoxide dismutases, catalases, and variuos peroxidases) as well as non-enzymatic antioxidants (e.g. glutathione, vitamins, and carotenoids) play a crucial role in protecting thyroid cells from an excess of ROS that are not used to produce thyroid hormones. In this way, their action serves as a protection against free radicals and guarantees an overall homeostasis [3–5]. However, an excessive amount of ROS can damage lipids, proteins, and DNA. In addition, they can negatively affected the physiologic adaptation and intra-cellular signal transduction, leading to an alteration of cellular homeostasis [6]. The imbalance between the ROS production and the detoxification system results in the cell oxidative stress (OS). Thyroid glands are characterized by numerous markers of OS, such as: (i) the prooxidant enzymes NADPH oxidases (NOX), which are an endogenous ROS source in thyroid tissue [7]; (ii) the Malondialdehyde (MDA), that is a product of lipid peroxidation by ROS, helping to evaluate the oxidative damage; (iii) others [2,3]. Different stages and types of thyroid diseases exhibit OS. In patients affected by hypothyroidism, a higher MDA amount has been observed in comparison with healthy individuals [6], probably due to a lower activity of the internal antioxidant system [8]. Similar condition has been noted for the autoimmune Hashimoto's thyroiditis, whose lesions lead to hypothyroidism [9]. High MDA level has also been detected in tissues collected from patients with toxic and non-toxic multinodular goiter [3]. At odds, in the hyperthyroidism condition, the overproduction of thyroid hormones results in the production of free radicals, which causes OS status [8], inducing damage to cell lipid membrane [10]. Oxidative DNA damage is believed to play a significant role in the pathogenesis of Graves' disease, which is the most common cause of hyperthyroidism [11].

In addition, several studies showed that increased OS levels are a relevant risk factor for both the beginning and progression of carcinogenesis [3,10,12–16]. In murine models, the thyroid gland is affected by oxidative damage more than other organs [17]. Also in patients affected by thyroid neoplasms, a higher DNA damage and serum ROS level have been reported compared to healthy control subjects [3,16]. Furthermore, the cancer thyroid tissues show modified metabolic pathways, aimed at enhancing the adaptability of cancer cells to unfavorable conditions. For instance, high OS condition promotes glycolysis. [3,12]. Notably, the oxidative profile of patients with papillary thyroid cancer (PTC) is worse than that of patients with autoimmune thyroid disease [18]. Besides, tumor differentiation has a negative correlation with OS, while the presence of somatic mutations has a positive correlation, as well as with the worst tumor presentation and higher tumor aggressiveness [16]. Finally, a recent in-vivo study evidenced that patients with thyroid cancer are characterized by an increased OS status [19].

Therefore, the connection between thyroid cancer diseases and oxidative stress is becoming prominent [3]. The OS balance depends primarily on mitochondrial functionality during cell respiration and on the cytochromes [20]. In detail, a key role is performed by cytochrome *c* (cyt *c*), which is an *α*-helical protein that folds around a covalently attached heme-Fe group and represents an integral component of the electron transport chain (ETC). The redox state of cyt *c*, i.e ferric (Fe^{3+}) or ferrous (Fe^{2+}) state, seems to be associated to its two different functions, which are the control of redox signaling in mitochondrial oxidative phosphorylation and the induction of apoptosis [21]. However, the redox state of cyt *c* is still a controversial topic. Another important and interesting part of ETC, for our purpose, is the Cu_A center of cytochrome oxidase and the *bc*1 complex (also named complex III), which is formed by cyt *b*, cytochrome *c*1 (cyt *c*1), and the Rieske iron-sulphur protein [22]. In particular, NOX (subunit of cyt*b*) is one of the major source of ROS during the transfer of the electrons to oxygen, as mentioned above [7]. Therefore, the redox state of mitochondrial cytochromes, in particular cyt *c* and cyt *b*, might be monitored as a versatile clinical tool [23]. Notably, choosing the specific laser excitation source that is in resonance with cytochromes vibrational modes, this effect can be exploited in resonance Raman scattering [20].

Finally, it is known that thyroid nodules are the predominant pathology of the endocrine system, that preferentially affects women. The detection of smaller nodules by ultra-sound (US) technique increases their incidence up to 19%–67% [24]. These lesions may have quite distinct nature, ranging from benign colloid nodules to malignant carcinoma. According to the current clinical guidelines, patients with doubtful US features or with large nodules undergo ultra sound-guided biopsy (fine needle aspiration, FNA), followed by cytological examination, in order to determine which patients have to be addressed to surgery [25]. Unfortunately, approximately 15%–20% of the cytological assessments falls within the indeterminate diagnostic category: in such cases, it is impossible to confirm or exclude the presence of carcinoma and part of these patients are referred for diagnostic surgery [26]. Notably, postoperative histological examination returns a diagnosis of benign for 70% of explanted thyroids [27]. In order to reduce this explorative surgery, it is mandatory to support cytological examination with other rapid and not invasive techniques. Among the available techniques, Raman spectroscopy (RS) is a good candidate, being a not invasive and label-free technique. As a matter of fact, vibrational spectroscopy, and in particular RS, has been successfully applied to cancer diagnosis of a variety of human tissues, such as breast [28], liver [29,30], colon [31,32], brain [20], oral cavity [33] and endometrium [34]. In recent years, our group proved that RS can discriminate between benign and malignant histological thyroid samples with an accuracy better than 90% [35–37]. Moreover, validation of RS as a diagnostic tool on cytological samples, i.e. on the thyroid FNA, as recommended by Trainor et al. [38] has been recently achieved [39], pointing out that RS could be used to understand the thyroid diseases. Indeed, cytological samples show a richer Raman profile compared to histological ones, likely related to the redox status of the samples.

The aim of this study is to find a correlation between RS features and OS status, by reporting the results on cytological thyroid samples from a cohort of 28 patients. These patients underwent thyroid FNA for nodular pathology, according to AME 2016 guidelines for clinic management of thyroid nodule [40] and received a second FNA after a time lapse of a few months. After the comparison among the Raman spectra collected from the first and the second FNA, these patients have been classified into 4 different categories. This classification has performed by the observation of oxidated/reduced cytochromes intensity ratio and the presence of carotenoids peaks [20,23]. Here, we report and comment the spectra of the most representative case for each category. The reported Raman analysis gives relevant information, not reported so far, to better understand disease development.

2. Materials and methods

2.1. Ethics statement

Our protocol adhered to the Declaration of Helsinki and to the International Conference on Harmonization Good Clinical Practice, and was approved by the Ethical Committee of Fondazione Policlinico Universitario Campus Bio-medico (FCBM), Rome (prot. 33.15 TS ComEt CBM and prot. 31/19 PAR ComEt CBM from July 26, 2019). All participants granted informed consent.

2.2. Patients enrollment

Patients afferent to the endocrinology outpatient clinic of FCBM for thyroid nodular pathology and with indication to FNA on the base of US features have been asked to participate in the study and to sign an informed consent form, approved by FCBM Ethical Committee.

Table 1
Category, cytological classification, Raman spectral features and clustering and histological diagnosis of the 5 most representative patients are reported. In particular, the letter (A, B, C, D, E) identifies the patient and the suffix -* (I, II) indicates the first or the second FNA, respectively. n.a. means not available, because patient is still in follow up.

Category	Patient ID	Cytological diagnostic category	Main Raman spectral features observed	Raman clustering	Histological diagnosis
1	A-I	TIR3A	Reduced Cytochromes *c* and *b*	Benign	
1	A-II	TIR3A	Oxidized and reduced Cytochromes *c* and *b*	Benign	n.a. Follow up
2	B-I	TIR1	Oxidized and reduced Cytochromes *c* and *b*	Benign	
2	B-II	TIR2	Oxidized and reduced Cytochromes *c* and *b*	Benign	Nodular hyperplasia
3	C-I	TIR2	Oxidized and reduced Cytochromes *c* and *b*	Benign	
3	C-II	TIR2	Oxidized and reduced Cytochromes *c* and *b* and Carotenoids	FV-PTC	NIFTP
4a	D-I	TIR5	Oxidized and reduced Cytochromes *c* and *b* and Carotenoids	FV-PTC	
4a	D-II	TIR5	Carotenoids and oxidized and reduced Cytochromes *c* and *b*	PTC	PTC
4b	E-I	TIR3B	Oxidized and reduced Cytochromes *c* and *b*	Benign	
4b	E-II	TIR3B	Carotenoids	PTC	PTC

2.3. Neck ultrasound, FNA and clinical evaluation

All subjects have been submitted to thyroid US evaluation, using a frequency range of 10 to 12 MHz on a MyLab 50 (Esaote, Genova, 144 Italy). US scan of thyroid gland and neck area have been performed by 2 experienced endocrinologists from FCBM. Nodules have been classified according to ACR TI-RADS risk stratification criteria [25]. In doubtful cases the endocrinologists conducted a separate session to reach an unified consensus. Demographic information, including age, gender, and family history of thyroid cancer and, laboratory data, regarding the thyroid function and the presence of autoimmune thyroiditis, were collected in an anonymized database.

2.4. Sample preparation

Cells have been sampled by FNA from thyroid nodules under US guidance. Part of this material has been smeared on microscopic slides and fixed with ethanol-based spray followed by Papanicolaou stain for routine cytological analysis. Diagnostic reports were described in agreement with Italian Consensus for Reporting Thyroid cytology [41]. The remaining cells have been directly spread on slides, without smearing or fixing, and stored at −80 ° C until Raman examination. All data and specimens have been anonymized according to the approved protocol.

2.5. Raman spectroscopy

Unpolarized Raman spectra have been collected by means of a Renishaw InVia Micro-Raman spectrometer. After a preliminary general view of the entire sample by 10x objective, we have selected ten different areas to be investigated by using 50x objective. In our setup, the laser beam from a solid-state diode laser source at 532 nm with a nominal output power of nearly 100 mW is focalized on the sample and the back-scattered intensity is collected through the spectrometer confocal microscope equipped with a Leica 50× LWD. A holographic edge filter provides high-contrast rejection of the elastically scattered light. Inelastically scattered intensity is instead dispersed by a diffraction grating (1800 grooves/mm) on a Peltier cooled 1024 × 256 pixel CCD detector. The final frequency resolution is of the order of 1 cm^{-1}. To prevent photo-damage, the laser power at the sample is controlled by neutral density filters. Punctual spectra (10 points per sample) have been collected in the extended scan mode, in the 100−3600 cm^{-1} range. At each point, 5 scans have been accumulated, corresponding to a total integration time of nearly 50 s.

Wire (Renishaw) software has been used to collect the raw spectra and perform the preliminary data reduction (e.g. background and fluorescence subtraction), while Matlab and Igor PRO softwares have been employed for the final analysis and normalization of each spectrum to its integral.

2.6. Study population

Twenty-eight patients, all undergoing to a first and second FNA during clinical follow-up, were enrolled in this specific monocentric study. Considering the evolution of Raman features between the two FNAs, the 28 patients have been pooled into 4 different categories. In particular, we present the most representative cases: case A for category 1; B for category 2; C for category 3; D for category 4 A; E for category 4B. Their clinical data, cytological results and Raman features have been summarized in Tables 1 and 2.

2.7. Statistical evaluation

Igor PRO and Origin softwares have been used for the statistical evaluation of the results. The theoretical and technical details along with the obtained outcomes are reported in Section 2 of Supplementary Materials.

3. Results and discussion

In a previous work [35], by applying RS to investigate histological samples from human thyroid, the presence of bands of carotenoids (~1003; ~1154 and ~1516 cm^{-1}) has been identified, as signature of cells affected by classical papillary carcinoma (PTC). In cells affected by the follicular variant of PTC (FV-PTC), the enhancement of the bands at 747; 1120 ÷ 1128; 1301 and 1585 cm^{-1}, along with the already quoted carotenoid ones, has been observed. These bands are assigned in the

Table 2
Clinical data of the 5 representative patients presented in this work. In particular, the letter (A, B, C, D, E) identifies the patient and the suffix -* (I, II) indicates the first or the second FNA, respectively.

Patient	Gender	Age	Cancer familiarity	Thyroid function	Thyroiditis	Nodule Dimensions (mm)	TIRADS (US)
A-I	M	49	No	Normal	No	6 × 7 × 9	4
A-II	M	49	No	Normal	No	6 × 7 × 9	4
B-I	M	55	No	Normal	No	25 × 28 × 42	4
B-II	M	55	No	Normal	No	33 × 32 × 42	4
C-I	F	67	No	Normal	No	20 × 33 × 33	4
C-II	F	67	No	Normal	No	20 × 33 × 38	4
D-I	F	78	No	Hyper-thyroidism	No	10 × 13 × 15	4
D-II	F	78	No	Hyper-thyroidism	No	10 × 13 × 15	4
E-I	F	72	No	Normal	Yes	10 × 10 × 10	4
E-II	F	72	No	Normal	Yes	8 × 12 × 12	4

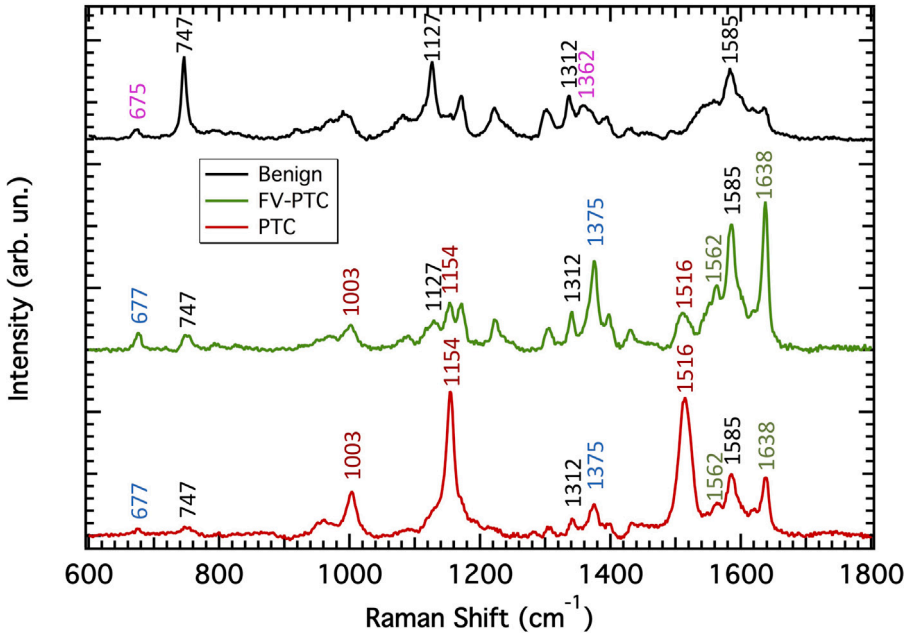

Fig. 1. Raman spectra collected on benign (black line), FV-PTC (green line) and PTC (red line) thyroid cells from FNA (single point, 50 s accumulation time). Spectra have been shifted for clarity. The Raman shifts of carotenoids are reported in red, those of oxidized and reduced cytochrome *c* are reported in green and black respectively, those of oxidized and reduced cytochrome *b* are reported in blue and magenta, respectively.

literature [42] to the vibrational modes of the heme proteins, namely cytochrome *c*, hemoglobin and myoglobin, among others. According to Refs. [35,39] and after our recent tests (see Supplementary Material for details), we assign these bands to cytochrome *c* (cyt *c*). Healthy thyroid tissues and benign samples (i.e. adenomas, hyperplasia) were instead characterized by the presence of the cyt *c* bands alone without carotenoid bands. These features, observed in histological sections, are preserved in cytological specimens.

Here, we present Raman spectra collected from thyroid FNA (see Fig. 1). All cytological samples show richer spectra in the fingerprint region (600-1800 cm^{-1}) in comparison with the histological ones. As a matter of fact, in cytological samples we can distinguish the characteristic bands of both reduced (747, 1127, 1312, 1585 cm^{-1}) and oxidized (1562, 1638 cm^{-1}) cyt *c* [23,43,44], along with those of reduced (675, 1362 cm^{-1}) and oxidized (677, 1375 cm^{-1}) cytochrome *b* (cyt *b*). In particular, the latter bands are ascribed to the NADPH oxydase subunit of cyt *b* [45]. For clarity, the assignments of each Raman peak are summarized in Table 3. The measured intensity ratio of the bands assigned to cyt *c* and *b* and carotenoids may change from one sample to another.

In order to investigate the evolution of the thyroid nodules, 28 patients have undergone to a second FNA, during follow up. The comparison of the Raman spectra collected from the cytological samples obtained by I FNA (Time zero) and II FNA evidences some differences due to the disease development. The most relevant and important variations are those associated to oxidated/reduced *cyt* c intensity ratio ($\Delta I_{1638}/I_{1585}$) and the carotenoid/reduced *cyt* c intensity ratio ($\Delta I_{1516}/I_{1585}$). For this reason, the 28 patients have been pooled into 4 different categories, according to RS features, as shown in the histogram of Fig. 2. The forth category is subdivided in 2 sub-classes,

Table 3
Raman peak assignment.

Raman shift (cm^{-1})	Assignment
675	reduced cyt *b*
677	oxidized cyt *b*
747	reduced cyt *c*
1003	carotenoids
1127	reduced cyt *c*
1154	carotenoids
1312	reduced cyt *c*
1362	reduced cyt *b*
1375	oxidized cyt *b*
1516	carotenoids
1562	oxidized cyt *c*
1585	reduced cyt *c*
1638	oxidized cyt *c*

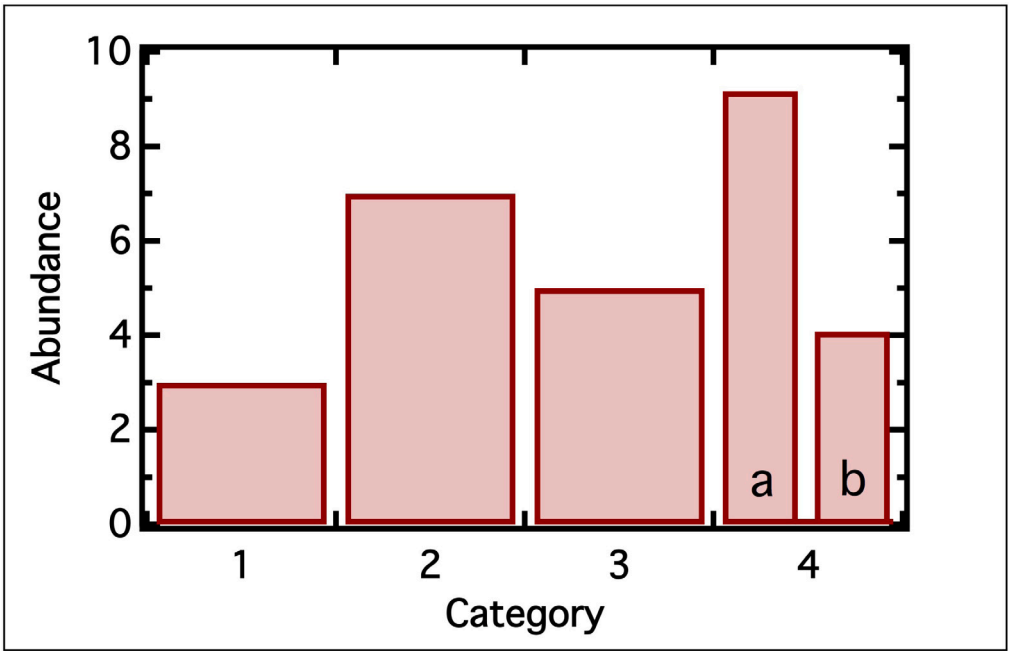

Fig. 2. Histogram of the investigated population (28 patients).

namely 4a and 4b for simplicity. The five most representative cases for each category and sub-category are reported.

In particular:

- Category 1 includes 3 patients with benign spectra in both FNAs, characterized by the increasing of oxidated cytochromes species in spite of reduced ones. In detail, valuing the I_{1638}/I_{1585} ratio, it is possible to observe a mean increasing of its value of about 60%. These patients are still in follow up or have received a benign histological diagnosis, in agreement with Raman clustering reported in Ref. [39]. This category is represented by the patient A.
- Category 2 counts 7 patients, in which the ratio oxidated/reduced cytochromes remains almost stable during follow up. The I_{1638}/I_{1585} ratio change is limited to no more than 5% in this class. This category is represented by the patient B.
- Category 3 contains 5 patients, characterized by the increasing of oxidated cytochromes species and the presence of carotenoids bands. In particular, the I_{1638}/I_{1585} ratio show an average growth of around 40%. This category is represented by the patient C.
- Category 4 involves 13 patients, marked by a significant increasing in intensity of the carotenoids spectral modes, for this reason also the intensity ratio I_{1516}/I_{1585} has been considered. This class is divided in two subclasses:
  - Category 4a, constituted by 9 patients, is characterized by a large enhancement of carotenoids features and a decreasing of the oxidated/reduced cytochromes ratio. In more details, the mean value of the I_{1638}/I_{1585} ratio decreases by approximately 25%, while the I_{1516}/I_{1585} ratio increases about 12 times from the first to second FNA, indicating the increase of the carotenoid feature. These patients have received mainly malignant diagnosis. This sub-category is represented by the patient D.
  - Category 4b includes 4 patients, showing a Raman spectrum more similar to benign one at I FNA and a malignant one at the time of II FNA. In this category, no change in the value of the I_{1638}/I_{1585} ratio has been observed, while a huge increase of about 60 times have been noted for the I_{1516}/I_{1585} ratio. All these patients have received a final malignant histological diagnosis. This sub-category is represented by the patient E.

To achieve a statistical significance evaluation of the variation in biomolecule content among the different categories, the Kruskal–Wallis test (H-test) has been performed on $\Delta I_{1638}/I_{1585}$ and $\Delta I_{1516}/I_{1585}$, followed by a non-parametric multiple comparison Dunn-Holland-Wolfe test (DHW-test). The H-tests return H=16.258, Hc=7.815, p-value= 1.0*10-3 for $\Delta I_{1638}/I_{1585}$ and H=21.484, Hc=7.815, p-value=8.3*10-5 for $\Delta I_{1516}/I_{1585}$ (details are reported in Table 1S and 2S in the supplementary material). Since both H values are higher respect to the threshold value Hc, we can assume a statistical significant difference in both features among two or more categories. To obtain an indication on which are the most significative variations among the categories, we have executed a multiple comparison test for each of the considered feature. The DHW tests (Table 3S and Table 4S in the supplementary material) reveal that, regarding the $\Delta I_{1638}/I_{1585}$, the most significant variations are between category 4 respect to category 3 and category 1, while for $\Delta I_{1516}/I_{1585}$, the most significant variations are between category 4 respect to category 1 and 2. In addition, the quadratic discriminant analysis (QDA), validated by a cross validation, was carried out (see Fig. 6S in the supplementary materials) in order to verify the presented classification, reported in Fig. 3. This analysis confirms the sorting into 4 categories observed in the clustering. The cross validation for training data indicates an error rate of 17.9%, conceivably due to the samples assignations of the samples to category 1 and category 3.

Evidences from RS are discussed in the light of the morphological features observed at microscope. The cytological diagnosis received by these patients (unchanged after follow up) is reported in Table 1, along with RS features. Additional clinical information is reported in Table 2.

Starting from the representative case of category 1, patient A (see Fig. 3), at time zero we observe a broad band, due to reduced cyt *c* centered at ~ 1585 cm^{-1}, showing two weak shoulders. Eight months later, this band develops two resolved peaks aside the central one: these new features (shown as green circles in Fig. 3) are assigned to oxidized cyt *c*. We notice also that the intensity of RS bands characteristic of reduced cyt *c* (blue stars in Fig. 3) decreases with time. Indeed, the value of the I_{1638}/I_{1585} ratio increases from the first and second FNA of about 115%. Moreover, the peak at 1362 cm^{-1}, assigned to reduced cyt *b*, disappears whereas the peak characteristic of oxidized cyt *b* (at

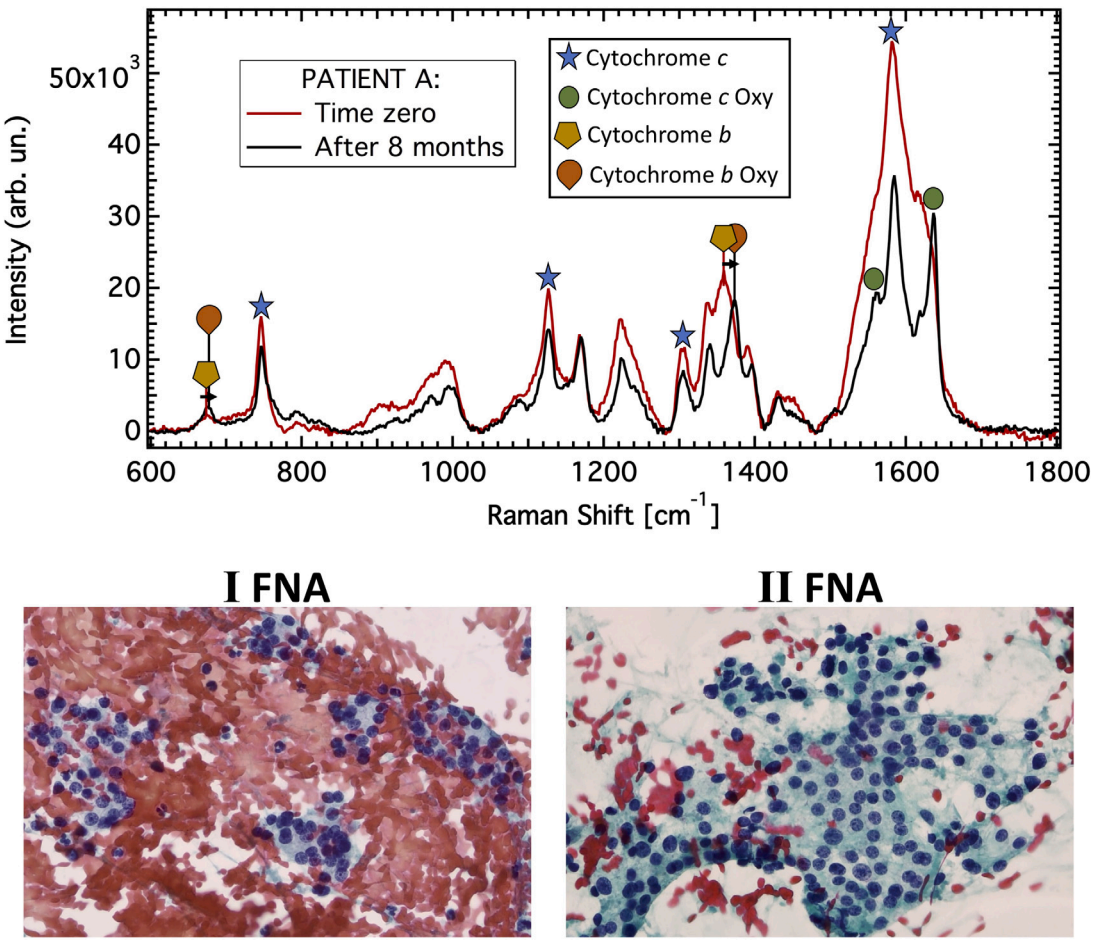

Fig. 3. Comparison between the spectra collected from patient A on two FNA samples. The red spectrum is recorded at time zero, the black one 8 months later. The blue stars label the lines assigned to reduced cyt *c* [35], the green circles label the lines assigned to the oxidized cyt *c* [43,44], the yellow pentagons label the lines characteristic of the reduced cyt *b* [45], and the orange drops label those assigned to the oxidized cyt *b* [45]. The microscope images of the I and II FNA slides are shown at the bottom (Papanicolaou Stain; original magnification 20x). I FNA: Thyrocytes with enlarged nuclei are organized in microfollicular pattern. Hematic background. II FNA: Thyrocytes with enlarged nuclei and visible nucleoli are organized in sheets and microfollicles. Poor colloid in background.

1375 cm^{-1}) shows up. The increased concentration of oxidized cyt *b* after 8 months is confirmed by the frequency shift along with intensity increase of the band at ~ 677 cm^{-1}. In both microscope images of the FNA slides (I FNA and II FNA shown in Fig. 3), similar modifications have been evidenced. These consist in architectural atypia with formation of a micro-follicular pattern and cellular alterations with thyrocytes characterized by enlarged nuclei and visible nucleoli in absence of nuclear clearing or grooves. Both FNA samples have received a cytological diagnosis of low risk indeterminate lesions (TIR3 A, Italian Consensus for Reporting Thyroid Cytology [41]). The RS clustering is benign in according to previous works [35,36], while the final histological diagnosis is not present because this patient continues the follow up. Nevertheless, all observed changes in Raman spectra suggest an increased oxidative stress levels during follow up, due to an imbalance of cellular homeostasis in favor of ROS production.

In the case of patient B (see Fig. 4), representative of category 2, at time zero we observe, in Amide I region, two resolved and intense peaks, placed at ~ 1562 and 1638 cm^{-1}, aside the central one, located at ~ 1585 cm^{-1}. These features are assigned to oxidized cyt *c* (green circles in Fig. 4) and reduced cyt *c* (blue star in Fig. 4), respectively. The other three peaks ascribable to reduced cyt *c* are also visible but with lower intensity compared to previously mentioned ones. In addition, there are also the two peaks referred to oxidized cyt *b* (at 677 and 1375 cm^{-1}). Eight months later, the spectral profile of the patient B remain almost stable in all features ($\Delta I_{1638}/I_{1585} \sim 4.8\%$) and the associated Raman clustering is benign [39]. Despite this, RS suggests a severe level of oxidative stress of cells during the follow up, as evidenced by the ratio between oxidated and reduced forms of cytochromes higher than 1 ($I_{1638}/I_{1585} \sim 1.17 \pm 0.06$) [23]. Cytological evaluation of the first FNA sample resulted not diagnostic (TIR 1) due to too low thyrocytes amount, which although benign, fail to meet the adequacy criteria. Indeed, in the microscope images of the I FNA slide, there are no groups of follicular cells, but only the presence of few foamy macrophages. Of note, RS clustering in this case resulted benign. Since the drop of FNA specimen used for RS was different from that one used for cytological evaluation, it is possible that the needle pass sample submitted for RS could be richer in thyrocytes compared with the smeared ones for cytological diagnosis. Conversely, the II FNA, that received a TIR 2 cytological diagnosis, shows follicular cells arranged in monolayer sheets and characterized by small round nuclei in a background of homogeneous colloid. The final histological diagnosis is nodular hyperplasia, confirming both the previous cytological examination and RS analysis.

In the case of patient C (see Fig. 5), representative of category 3, the collected spectra from the two FNA show a quite distinct development of the nodule compared to those of previous analyzed categories. In

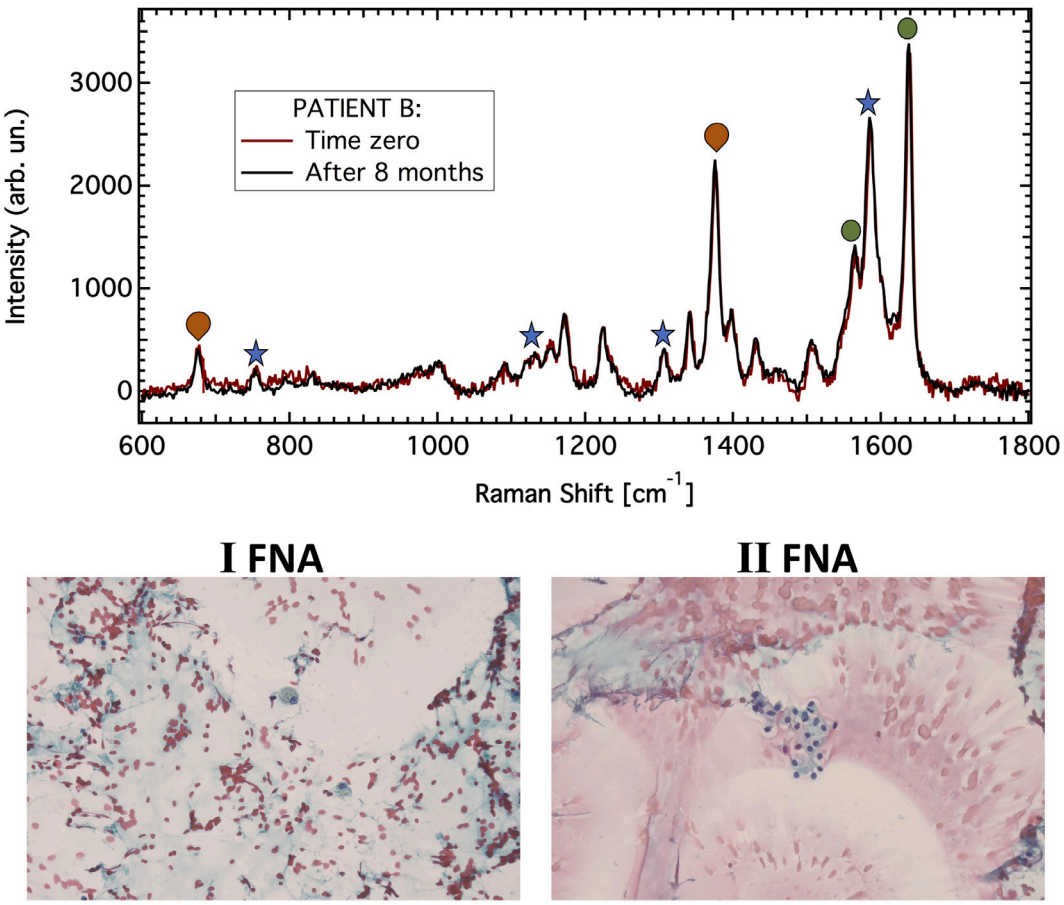

Fig. 4. Comparison between the spectra collected from patient B on two FNA samples. Red spectrum has been collected at time zero, the black one during a second FNA performed 8 months later, as reported in the legend. Symbols for the assignment of peaks to specific components are the same as for Fig. 3. The microscope images of the I and II FNA slides are shown at the bottom (Papanicolaou Stain; original magnification 10x). I FNA: there are no thyrocytes on the cytological slide, only few foamy macrophages are present. II FNA: A group of thyrocytes with small round nuclei are present in a background of homogeneous colloid.

detail, while cells at time zero show only the bands assigned to cyt *c* and *b* (both reduced and oxidized), the spectrum collected 8 months later evidences also the presence of carotenoids. These features are similar to those observed for FV-PTC samples [35,37]. In addition, we notice the increase of the intensity ratio between bands of oxidized/reduced cytochromes ($\Delta I_{1638}/I_{1585} \sim +85\%$). The cytological diagnostic category of this patient was benign (TIR2) in both the FNAs. The I FNA slide shows watery colloid with cracking artefacts and a few thyrocytes with round, small nuclei, typical of benign tissues. The II FNA slide shows a larger number of thyrocytes assembled in follicular sheet pattern in a colloid background. Although cells are crowded, the follicular group is uniform and presents regular borders. Indeed, this patient underwent surgery due to compressive symptoms and, after surgery, the histological diagnosis was Non-invasive Follicular Thyroid Neoplasm with Papillary-like Nuclear Features (NIFTP) [46,47], that is a non-invasive stage of PTC disease. Thus, our data suggest that the Raman spectrum of NIFTP cells is similar to that of FV-PTC one. Here, carotenoids uptake may be activated in order to mitigate the ROS increasing and their negative effects on the cells, as suggested by the intensity ratio of the peaks assigned to oxidized/reduced cytochromes. At this stage the malignant neoplastic transformation already started. NIFTP is a recently introduced diagnosis in thyroid tumors [46] and the new WHO thyroid tumors classification put NIFTP in the low risk thyroid neoplasms group, underlining the inter-observer variability and the usual benign clinical behavior [48]. Cytological identification of this entity is not possible on the morphological ground [49] and such cases usually fall in the indeterminate categories. In our case the final histological diagnosis showed a macrofollicular NIFTP, so giving a false negative picture due to colloid prevalent smears in the cytological samples. Herein we may argue that RS may be more informative about the relation among OS, carotenoids function and disease clustering, than the standard cytological examination.

Focusing our attention on category 4, we present and discuss the representative cases of each sub-classes. In the case of patient D (see Fig. 6), that belongs and represents class 4a, spectra show the signatures of both cytochromes and carotenoids. The intensity of the carotenoid bands is very low at time zero and clearly increases after 3 months. In particular, these grow of approximately 12 times. In both spectra we notice that the signatures of reduced cyt *b* are not visible, while the intensity of the peaks assigned to reduced cyt *c* (blue stars in Fig. 6) increases with time with a concomitant intensity reduction of the peaks assigned to oxidated cyt *c*. Thus, the value of the I_{1638}/I_{1585} ratio decreases of about 25%. The latter effect may be due to the uptake of carotenoids, exploiting their antioxidant function [50]. This could be an example of carotenoids used by cancerous cells to survive themselves, as the oxidative stress is decreased, avoiding cells apoptosis [12]. The above mentioned spectral features of the II FNA insert this patient in the PTC Raman cluster [39]. The cytological diagnosis for this patient was malignant (TIR5), with PTC features. Due to relevant comorbidities, the patient was not immediately addressed to surgery. After a period of active follow up, a second FNA was performed aimed to molecular assessment, showing BRAFV600E mutation. Considering the diagnosis,

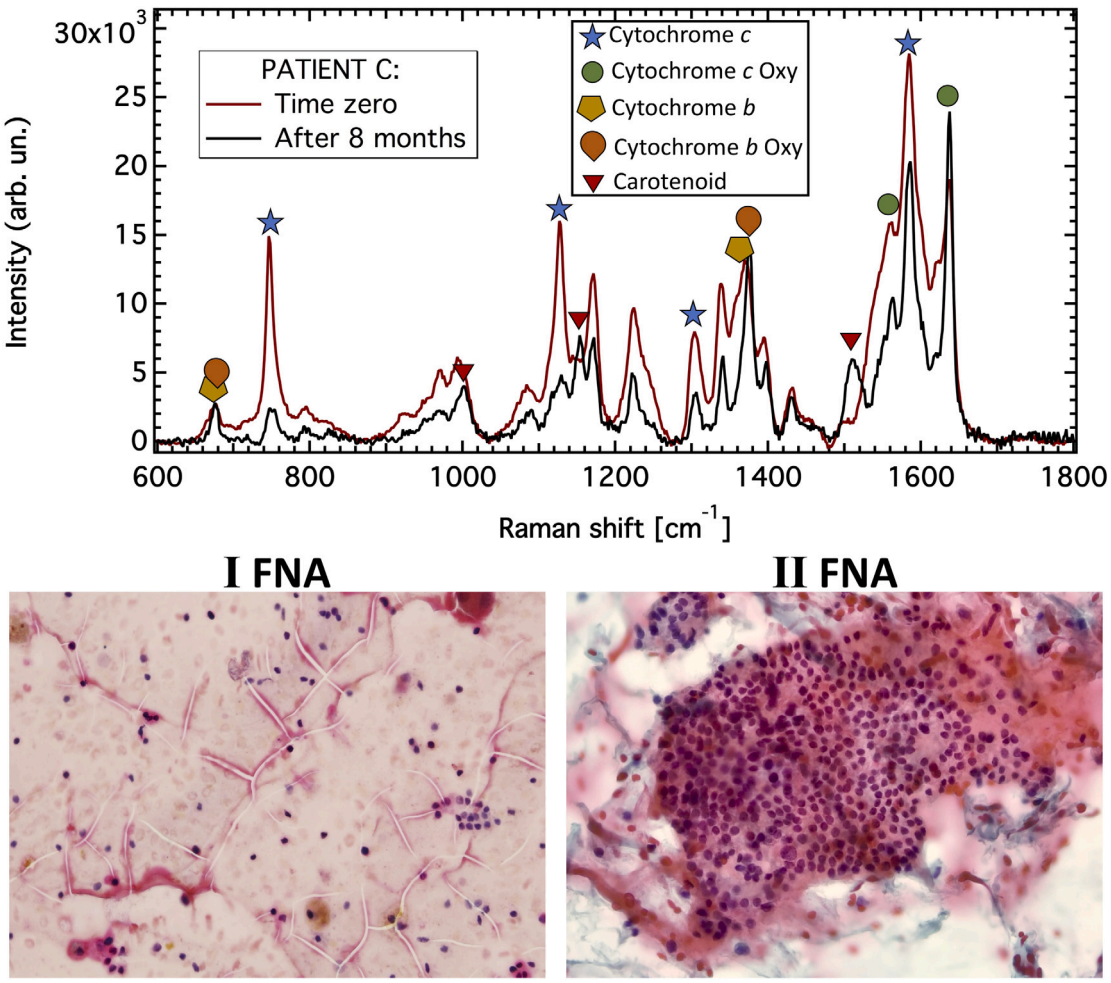

Fig. 5. Comparison between the spectra collected from patient C on two FNA samples. Red spectrum has been collected at time zero, the black one during a second FNA performed a few monthes later, as reported in the legend. Symbols for the assignment of peaks to specific components of the aspirate are the same as for Fig. 3; red triangles label the lines assigned to carotenoids [35]. The microscope images of the I and II FNA slides are shown at the bottom (Papanicolaou Stain; original magnification 10x). I FNA: Few groups of thyrocytes with small round nuclei are present in a background of homogeneous colloid with foamy macrophages. II FNA: A flat sheet of thyrocytes showing regular borders is evident in a colloid background.

the molecular result, and the hyperthyroidism, a total thyroidectomy was performed with the expected histological diagnosis of PTC, in agreement with cytological diagnosis and the RS clustering [39]. As a matter of fact, the I FNA slide shows a three dimensional group of atypical thyrocytes with nuclear overlapping, grooves and small peripherical nucleoli. In the II FNA slide the morphological features typical of PTC are better represented: we notice thyrocytes with enlarged and oval nuclei, grooves and nuclear pseudo-inclusions. Atypical thyrocytes are arranged in groups with digitate profile reflecting the papillary architecture of classical PTC.

Finally, the representative case of 4b class is identified by patient E (see Fig. 7). The collected spectra from the two FNA show a change from a benign-like spectrum at time zero to a PTC spectrum after 5 months. Indeed, in the latter spectrum only the carotenoid peaks are visible. Despite this change in RS clustering [39], the cytological diagnosis was TIR3B (high-risk indeterminate lesions) in both the FNAs. We notice that in this case the comparison between the I FNA slide and the II one shows less evident changes between the two pictures, being both characterized by enlarged nuclei, focal nuclear clearing, prominent nucleoli and light eosinophilic cytoplasm (Fig. 7). These atypical features suspicious for neoplasia, are sometimes present in lymphocytic thyroiditis, as in the case of this patients. This event represents a challenging diagnostic issue since the nuclear atypia may be the result of inflammatory disease so leading to an indeterminate cytological category [51]. In agreement with international guidelines for thyroid nodules, this patient was submitted for surgery with a final histological diagnosis of encapsulated invasive follicular variant of PTC in a Hashimoto thyroiditis background. Raman clustering confirms the histological diagnosis [39]. The absence of carotenoids in the spectrum from the I FNA may be probably due to a lymphocytic predominance in the cytological drop evaluated for Raman assessment and needs a further investigation.

Our results show that RS seems informative about the cells redox status and different development state of thyroid nodules. The difficult in knowing the cellular composition of the specimen drop submitted to RS analysis is currently the limit of the study. Future perspective will require a new model of analysis able to compare morphological and spectroscopic evaluation on the same sample. To date, the evidences of this study fit with the model of tumorigenesis presented so far in the literature [3,12,16].

4. Conclusions

Oxidative stress is mentioned as one of the major risks factor in pathological disease and cancer [3,12,14]. Of relevance, recent

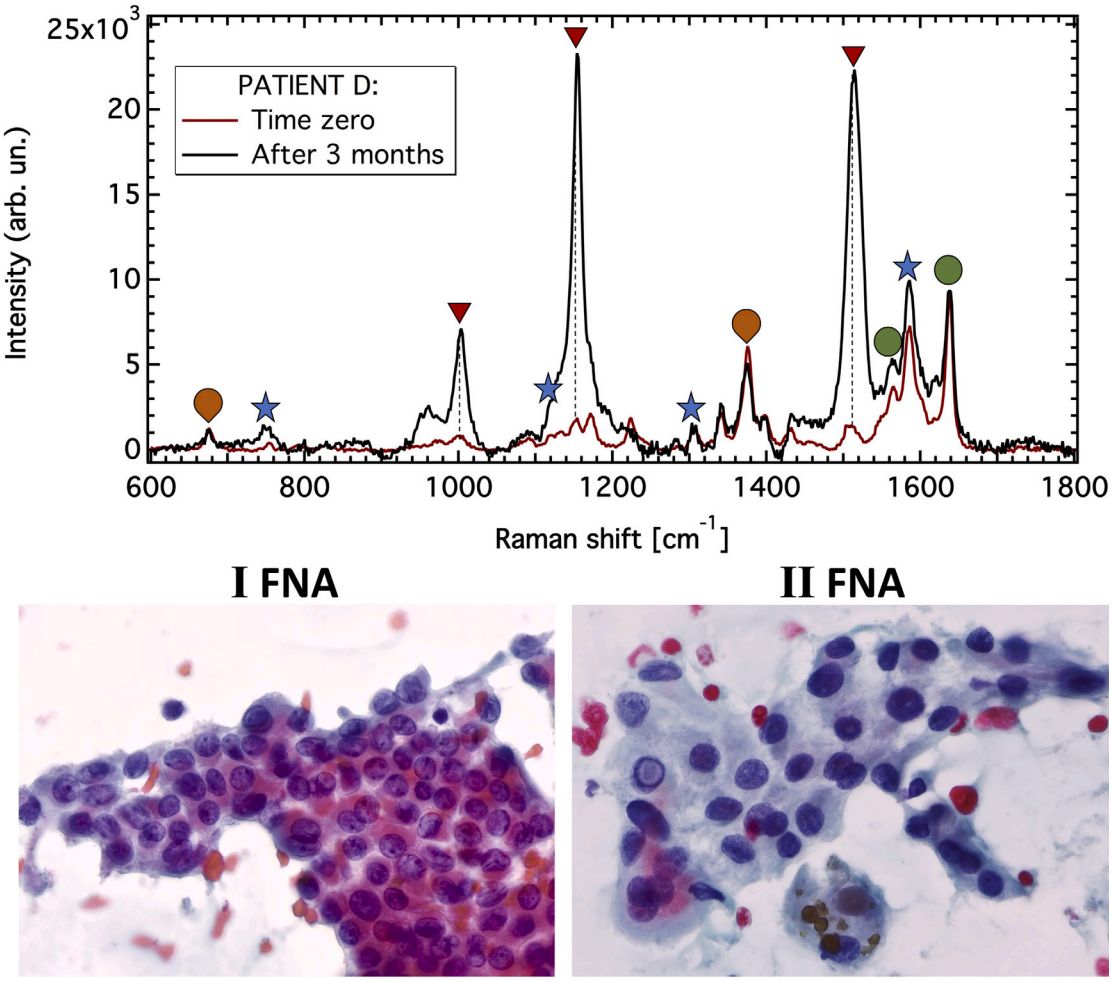

Fig. 6. Comparison between the spectra collected from patient D on two FNA samples. Red spectrum has been collected at time zero, the black one during a second FNA performed a few months later, as reported in the legend. Symbols for the assignment of peaks to specific components of the aspirate are the same as for Fig. 5. The microscope images of the I and II FNA slides are shown at the bottom (Papanicolaou Stain; original magnification 40x). I FNA: A threedimensional group of atypical thyrocytes shows nuclear overlapping, grooves, and small peripherical nucleoli. II FNA: Thyrocytes with enlarged irregular nuclei, grooves and nuclear pseudoinclusion are arranged in a group with digitate profile.

data explored the relation of mutational status and tumor behavior with OS suggesting that OS correlates with tumor aggressiveness and mutations in the MEK-ERK pathway in PTC [16]. In this study, our results confirm that high levels of ROS impact on thyroid cancerous cell, probably acting on tumor pathogenesis. It is known that thyroid epithelial cells physiologically produce moderate amounts of ROS for thyroid hormonogenesis, so thyrocytes need constantly to balance their metabolism against excessive ROS production [1]. All investigated samples highlight a strong correlation between OS status, uptake of carotenoids and/or thyroid disease development.

We have pointed out that RS is, among the available biomarkers of oxidative stress, a sensible tool in order to measure OS levels and to facilitate an earlier cancer diagnosis on FNA combined with the traditional examination. In addition, assessing OS status may give relevant and important information to better understand the degree of the thyroid cancer development and also the associated risk assessment.

Future efforts will be enlarging the study population and extending RS analysis during the patient follow up in association with morphological correlation. In conclusion, the present study paves the way to fundamental research on new signaling pathways and biomarkers involved in cell OS, which influences the thyroid disease and cancer development.

Declaration of competing interest

The authors declare that they have no known competing financial interests or personal relationships that could have appeared to influence the work reported in this paper.

Data availability

The authors do not have permission to share data.

Acknowledgments

The Authors acknowledge financial support from Ministero della Salute, Italy through the TIRAMA project (RF-2018-12366568) and IDRA project (PNRR-POC-2022-12376531). The authors acknowledge the Rome Technopole Innovation Ecosystem Foundation, Italy (PNRR grant M4-C2-Inv. 1.5 F83B22000040006). MDG, AP, AS, MAR gratefully acknowledge the Grant of Excellent Departments 2023-2027, MUR (ARTICOLO 1, COMMI 314-337, LEGGE 232/2016).

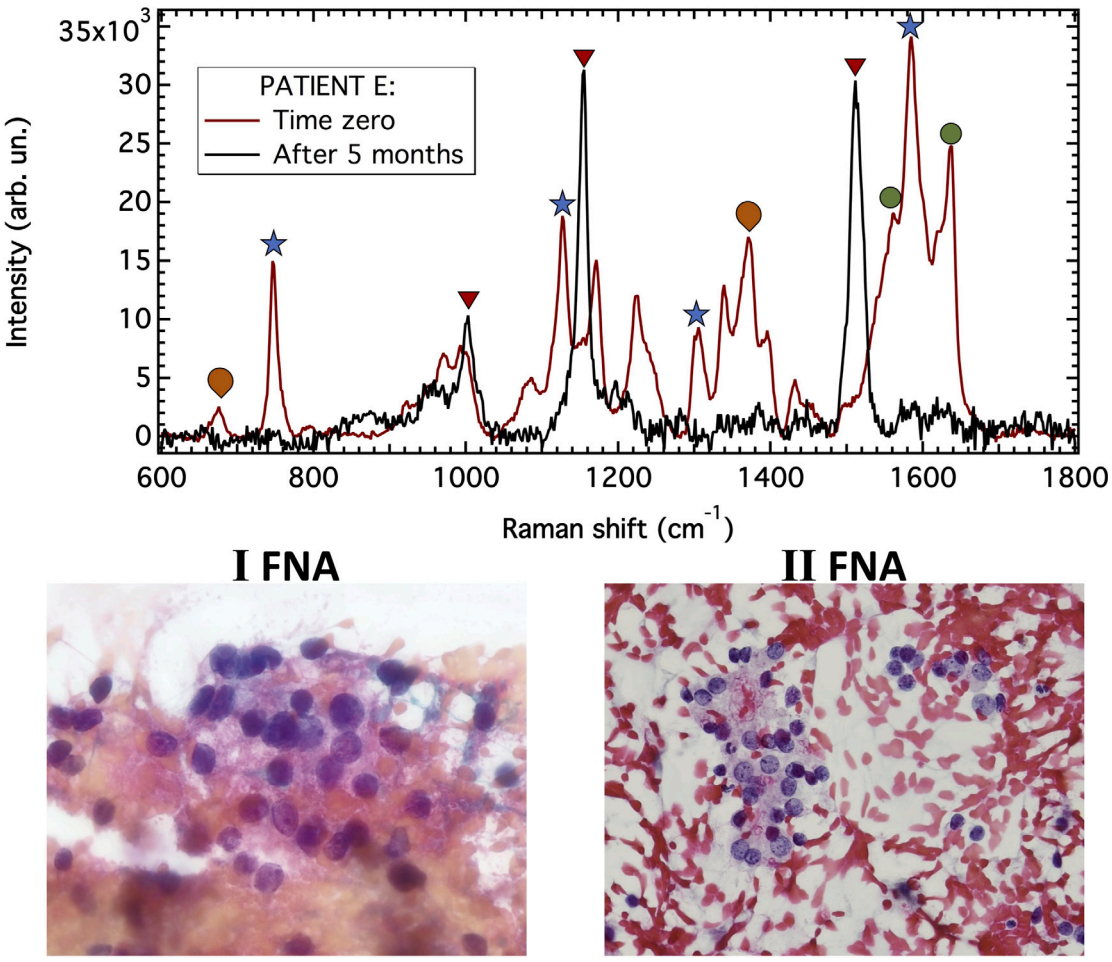

Fig. 7. Comparison between the spectra collected from patient E on two FNA samples. Red spectrum has been collected at time zero, the black one during a second FNA performed a few months later, as reported in the legend. Symbols for the assignment of peaks to specific components of the aspirate are the same as for Fig. 5. The microscope images of the I and II FNA slides are shown at the bottom (Papanicolaou Stain; original magnification 20x). I FNA: Thyrocytes with enlarged nuclei, focal nuclear overlapping and prominent nucleoli show eosinophilic cytoplasm. II FNA: Thyrocytes present enlarged nuclei, focal nuclear clearing, prominent nucleoli and light eosinophilic cytoplasm. No colloid in background.

Appendix A. Supplementary data

Supplementary material related to this article can be found online at https://doi.org/10.1016/j.saa.2024.125206.

References

[1] S. Poncin, A.-C. Gérard, M. Boucquey, M. Senou, P.B. Calderon, B. Knoops, B.t. Lengelé, M.-C. Many, I.M. Colin, Oxidative stress in the thyroid gland: From harmlessness to hazard depending on the iodine content, Endocrinology 149 (1) (2008) 424–433, http://dx.doi.org/10.1210/en.2007-0951, arXiv:https://academic.oup.com/endo/article-pdf/149/1/424/8995175/endo0424.pdf.

[2] M.T. Macvanin, Z. Gluvic, S. Zafirovic, X. Gao, M. Essack, E.R. Isenovic, The protective role of nutritional antioxidants against oxidative stress in thyroid disorders, Front. Endocrinol. 13 (2023) http://dx.doi.org/10.3389/fendo.2022.1092837, URL https://www.frontiersin.org/articles/10.3389/fendo.2022.1092837.

[3] J. Kochman, K. Jakubczyk, P. Bargiel, K. Janda-Milczarek, The influence of oxidative stress on thyroid diseases, Antioxidants 10 (9) (2021) http://dx.doi.org/10.3390/antiox10091442, URL https://www.mdpi.com/2076-3921/10/9/1442.

[4] W. Stahl, H. Sies, Antioxidant activity of carotenoids, Mol. Aspects Med. 24 (6) (2003) 345–351, http://dx.doi.org/10.1016/S0098-2997(03)00030-X, URL https://www.sciencedirect.com/science/article/pii/S009829970300030X, Fat Soluble Vitamins: Old Molecules with Novel Properties.

[5] A. di Masi, R.L. Sessa, Y. Cerrato, G. Pastore, B. Guantario, R. Ambra, M. Di Gioacchino, A. Sodo, M. Verri, P. Crucitti, F. Longo, A.M. Naciu, A. Palermo, C. Taffon, F. Acconcia, F. Bianchi, P. Ascenzi, M.A. Ricci, A. Crescenzi, Unraveling the effects of carotenoids accumulation in human papillary thyroid carcinoma, Antioxidants 11 (8) (2022) http://dx.doi.org/10.3390/antiox11081463, URL https://www.mdpi.com/2076-3921/11/8/1463.

[6] S.K. Chakrabarti, S. Ghosh, S. Banerjee, S. Mukherjee, S. Chowdhury, Oxidative stress in hypothyroid patients and the role of antioxidant supplementation, Indian J. Endocrinol. Metabol. 20 (5) (2016) 674.

[7] H. Ohye, M. Sugawara, Dual oxidase, hydrogen peroxide and thyroid diseases, Exp. Biol. Med. 235 (4) (2010) 424–433, http://dx.doi.org/10.1258/ebm.2009.009241.

[8] A. Mancini, C. Di Segni, S. Raimondo, G. Olivieri, A. Silvestrini, E. Meucci, D. Currò, et al., Thyroid hormones, oxidative stress, and inflammation, Mediators Inflamm. 2016 (2016).

[9] I. Ates, M.F. Arikan, M. Altay, F.M. Yilmaz, N. Yilmaz, D. Berker, S. Guler, The effect of oxidative stress on the progression of Hashimoto's thyroiditis, Arch. Physiol. Biochem. 124 (4) (2018) 351–356.

[10] D. Wang, J.-F. Feng, P. Zeng, Y.-H. Yang, J. Luo, Y.-W. Yang, Total oxidant/antioxidant status in sera of patients with thyroid cancers, Endocrine-Related Cancer 18 (6) (2011) 773–782, http://dx.doi.org/10.1530/ERC-11-0230, URL https://erc.bioscientifica.com/view/journals/erc/18/6/773.xml.

[11] S. De Leo, S.Y. Lee, L.E. Braverman, Hyperthyroidism, Lancet 388 (10047) (2016) 906–918.

[12] C. Gorrini, I.S. Harris, T.W. Mak, Modulation of oxidative stress as an anticancer strategy, Nat. Rev. Drug Discov. 12 (12) (2013) 931–947, http://dx.doi.org/10.1038/nrd4002.

[13] Y. Luo, J. Ma, W. Lu, The significance of mitochondrial dysfunction in cancer, Int. J. Mol. Sci. 21 (16) (2020) http://dx.doi.org/10.3390/ijms21165598, URL https://www.mdpi.com/1422-0067/21/16/5598.

[14] J.D. Hayes, A.T. Dinkova-Kostova, K.D. Tew, Oxidative stress in cancer, Cancer Cell 38 (2) (2020) 167–197, http://dx.doi.org/10.1016/j.ccell.2020.06.001, URL https://www.sciencedirect.com/science/article/pii/S1535610820302749.

[15] C.S. Palmer, A.J. Anderson, D. Stojanovski, Mitochondrial protein import dysfunction: Mitochondrial disease, neurodegenerative disease and cancer, FEBS Lett. 595 (8) (2021) 1107–1131, http://dx.doi.org/10.1002/1873-3468.14022, arXiv:https://febs.onlinelibrary.wiley.com/doi/pdf/10.1002/1873-3468.14022, URL https://febs.onlinelibrary.wiley.com/doi/abs/10.1002/1873-3468.14022.

[16] M. Muzza, G. Pogliaghi, C. Colombo, E. Carbone, V. Cirello, S. Palazzo, F. Frattini, D. Gentilini, G. Gazzano, L. Persani, L. Fugazzola, Oxidative stress correlates with more aggressive features in thyroid cancer, Cancers 14 (23) (2022) http://dx.doi.org/10.3390/cancers14235857, URL https://www.mdpi.com/2072-6694/14/23/5857.

[17] J. Maier, H. van Steeg, C. van Oostrom, S. Karger, R. Paschke, K. Krohn, Deoxyribonucleic acid damage and spontaneous mutagenesis in the thyroid gland of rats and mice, Endocrinology 147 (7) (2006) 3391–3397, http://dx.doi.org/10.1210/en.2005-1669, arXiv:https://academic.oup.com/endo/article-pdf/147/7/3391/9031198/endo3391.pdf.

[18] S. Lassoued, M. Mseddi, F. Mnif, M. Abid, F. Guermazi, H. Masmoudi, A. El Feki, H. Attia, A comparative study of the oxidative profile in Graves' disease, Hashimoto's thyroiditis, and papillary thyroid cancer, Biol. Trace Element Res. 138 (2010) 107–115.

[19] M. Kosciuszko, A. Buczynska, A.J. Kretowski, A. Poplawska-Kita, Could oxidative stress play a role in the development and clinical management of differentiated thyroid cancer? Cancers 15 (12) (2023) http://dx.doi.org/10.3390/cancers15123182, URL https://www.mdpi.com/2072-6694/15/12/3182.

[20] H. Abramczyk, B. Brozek-Pluska, M. Kopec, J. Surmacki, M. Blaszczyk, M. Radek, Redox imbalance and biochemical changes in cancer by probing redox-sensitive mitochondrial cytochromes in label-free visible resonance Raman imaging, Cancers 13 (5) (2021) 960, http://dx.doi.org/10.3390/cancers13050960, URL https://www.mdpi.com/2072-6694/13/5/960.

[21] D.L. Mendez, I.V. Akey, C.W. Akey, R.G. Kranz, Oxidized or reduced cytochrome c and axial ligand variants all form the apoptosome in vitro, Biochemistry 56 (22) (2017) 2766–2769, http://dx.doi.org/10.1021/acs.biochem.7b00309, PMID: 28510448.

[22] M.O. Ripple, M. Abajian, R. Springett, Cytochrome c is rapidly reduced in the cytosol after mitochondrial outer membrane permeabilization, Apoptosis 15 (2010) 563–573, http://dx.doi.org/10.1007/s10495-010-0455-2.

[23] H. Xie, L. Song, S. Katz, J. Zhu, Y. Liu, J. Tang, L. Cai, P. Hildebrandt, X.X. Han, Electron transfer between cytochrome c and microsomal monooxygenase generates reactive oxygen species that accelerates apoptosis, Redox Biol. 53 (2022) 102340, http://dx.doi.org/10.1016/j.redox.2022.102340, URL https://www.sciencedirect.com/science/article/pii/S2213231722001124.

[24] P. Bérard, G. Besson, D.S. Gallot, G.M. Doherty, B.R. Haugen, R.T. Kloos, S.L. Lee, S.J. Mandel, E.L. Mazzaferri, B. McIver, F. Pacini, M. Schlumberger, S.I. Sherman, D.L. Steward, R.M. Tuttle, Revised American thyroid association management guidelines for patients with thyroid nodules and differentiated thyroid cancer, Thyroid 19 (11) (2009) 1167–1214, http://dx.doi.org/10.1089/thy.2009.0110.

[25] F.N. Tessler, W.D. Middleton, E.G. Grant, J.K. Hoang, L.L. Berland, S.A. Teefey, J.J. Cronan, M.D. Beland, T.S. Desser, M.C. Frates, L.W. Hammers, U.M. Hamper, J.E. Langer, C.C. Reading, L.M. Scoutt, A.T. Stavros, ACR Thyroid Imaging, Reporting and Data System (TI-RADS): White paper of the ACR TI-RADS Committee, J. Am. College Radiol. 14 (5) (2017) 587–595, http://dx.doi.org/10.1016/j.jacr.2017.01.046.

[26] H. Gharib, E. Papini, J.R. Garber, D.S. Duick, R.M. Harrell, L. Hegedus, R. Paschke, R. Valcavi, P. Vitti, American Association of Clinical Endocrinologists, American College of Endocrinology, and Associazione Medici Endocrinologi Medical Guidelines for Clinical Practice for the Diagnosis and Management of Thyroid Nodules - 2016 Update Appendix, Endocrine Pract. 22 (2016) 1–60, http://dx.doi.org/10.4158/EP161208.GL, URL https://www.sciencedirect.com/science/article/pii/S1530891X20429544, American Association of Clinical Endocrinologists, American College of Endocrinology, and Associazione Medici Endocrinologi Medical Guidelines for Clinical Practice for the Diagnosis and Management of Thyroid Nodules - 2016 Update Appendix.

[27] S.E. Titov, E.S. Kozorezova, P.S. Demenkov, Y.A. Veryaskina, I.V. Kuznetsova, S.L. Vorobyev, R.A. Chernikov, I.V. Sleptsov, N.I. Timofeeva, M.K. Ivanov, Preoperative typing of thyroid and parathyroid tumors with a combined molecular classifier, Cancers 13 (2) (2021) 237, http://dx.doi.org/10.3390/cancers13020237, URL https://www.mdpi.com/2072-6694/13/2/237.

[28] H. Abramczyk, B. Brozek-Pluska, New look inside human breast ducts with Raman imaging. Raman candidates as diagnostic markers for breast cancer prognosis: Mammaglobin, palmitic acid and sphingomyelin, Anal. Chim. Acta 909 (2016) 91–100, http://dx.doi.org/10.1016/j.aca.2015.12.038, URL https://www.sciencedirect.com/science/article/pii/S0003267016300149.

[29] R. Di Santo, M. Vaccaro, S. Romanò, F. Di Giacinto, M. Papi, G.L. Rapaccini, M. De Spirito, L. Miele, U. Basile, G. Ciasca, Machine learning-assisted FTIR analysis of circulating extracellular vesicles for cancer liquid biopsy, J. Personal. Med. 12 (6) (2022) http://dx.doi.org/10.3390/jpm12060949, URL https://www.mdpi.com/2075-4426/12/6/949.

[30] L. Huang, H. Sun, L. Sun, K. Shi, Y. Chen, X. Ren, Y. Ge, D. Jiang, X. Liu, W. Knoll, et al., Rapid, label-free histopathological diagnosis of liver cancer based on Raman spectroscopy and deep learning, Nature Commun. 14 (1) (2023) 48.

[31] H. Noothalapati, K. Iwasaki, T. Yamamoto, Non-invasive diagnosis of colorectal cancer by Raman spectroscopy: Recent developments in liquid biopsy and endoscopy approaches, Spectrochimica Acta A 258 (2021) 119818, http://dx.doi.org/10.1016/j.saa.2021.119818, URL https://www.sciencedirect.com/science/article/pii/S1386142521003942.

[32] S. Romanò, F. Di Giacinto, A. Primiano, J. Gervasoni, A. Mazzini, M. Papi, A. Urbani, A. Serafino, M. De Spirito, E.K. Krasnowska, G. Ciasca, Label-free spectroscopic characterization of exosomes reveals cancer cell differentiation, Anal. Chim. Acta 1192 (2022) 339359, http://dx.doi.org/10.1016/j.aca.2021.339359, URL https://www.sciencedirect.com/science/article/pii/S0003267021011855.

[33] O. Ibrahim, M. Toner, S. Flint, H.J. Byrne, F.M. Lyng, The potential of Raman spectroscopy in the diagnosis of dysplastic and malignant oral lesions, Cancers 13 (4) (2021) 619, http://dx.doi.org/10.3390/cancers13040619, URL https://www.mdpi.com/2072-6694/13/4/619.

[34] J. Depciuch, E. Barnas, J. Skret-Magierlo, A. Skret, E. Kaznowska, K. Łach, P. Jakubczyk, J. Cebulski, Spectroscopic evaluation of carcinogenesis in endometrial cancer, Sci. Rep. 11 (2021) 9079–9091, http://dx.doi.org/10.1038/s41598-021-88640-7.

[35] M. Sbroscia, M. Di Gioacchino, P. Ascenzi, P. Crucitti, A. di Masi, I. Giovannoni, F. Longo, D. Mariotti, A.M. Naciu, A. Palermo, C. Taffon, M. Verri, A. Sodo1, A. Crescenzi, M.A. Ricci, Thyroid cancer diagnosis by Raman spectroscopy, Sci. Rep. 10 (2020) 91–100, http://dx.doi.org/10.1038/s41598-020-70165-0.

[36] A. Sodo, M. Verri, A. Palermo, A.M. Naciu, M. Sponziello, C. Durante, M. Di Gioacchino, A. Paolucci, A. di Masi, F. Longo, P. Crucitti, C. Taffon, M.A. Ricci, A. Crescenzi, Raman spectroscopy discloses altered molecular profile in thyroid adenomas, Diagnostics (Basel) 11 (2020) 43–54, http://dx.doi.org/10.3390/diagnostics11010043.

[37] L. Bellantuono, R. Tommasi, E. Pantaleo, M. Verri, N. Amoroso, P. Crucitti, M. Di Gioacchino, F. Longo, A. Monaco, A.M. Naciu, et al., An eXplainable Artificial Intelligence analysis of Raman spectra for thyroid cancer diagnosis, Sci. Rep. 13 (1) (2023) 16590, http://dx.doi.org/10.1038/s41598-023-43856-7.

[38] D. Traynor, I. Behl, D. O'Dea, F. Bonnier, S. Nicholson, F. O'Connell, A. Maguire, S. Flint, S. Galvin, C.M. Healy, et al., Raman spectral cytopathology for cancer diagnostic applications, Nat. Protoc. (2021) 1–20.

[39] A. Palermo, A. Sodo, A.M. Naciu, M. Di Gioacchino, A. Paolucci, A. di Masi, D. Maggi, P. Crucitti, F. Longo, E. Perrella, C. Taffon, M. Verri, M.A. Ricci, A. Crescenzi, Clinical Use of Raman spectroscopy improves diagnostic accuracy for indeterminate thyroid nodules, J. Clin. Endocrinol. Metabol. (2022) http://dx.doi.org/10.1210/clinem/dgac537, arXiv:https://academic.oup.com/jcem/advance-article-pdf/doi/10.1210/clinem/dgac537/46223849/dgac537.pdf, dgac537.

[40] M. Hossein Gharib, M. Enrico Papini, J.R. Garber, D.S. Duick, R.M. Harrell, L. Hegedüs, R. Paschke, M. Roberto Valcavi, P. Vitti, et al., American Association of clinical Endocrinologists, American College of Endocrinology, and Associazione Medici Endocrinologi Medical Guidelines for Clinical Practice for the Diagnosis and Management of thyroid Nodules-2016 update executive summary of recommendations, Endocrine Pract. 22 (5) (2016) 622.

[41] F. Nardi, F. Basolo, A. Crescenzi, G. Fadda, A. Frasoldati, F. Orlandi, L. Palombini, E. Papini, M. Zini, A. Pontecorvi, et al., Italian consensus for the classification and reporting of thyroid cytology, J. Endocrinol. Investig. 37 (2014) 593–599.

[42] A. Rygula, K. Majzner, K.M. Marzec, A. Kaczor, M. Pilarczyk, M. Baranska, Raman spectroscopy of proteins: A review, J. Raman Spectrosc. 44 (8) (2013) 1061–1076, http://dx.doi.org/10.1002/jrs.4335, arXiv:https://analyticalsciencejournals.onlinelibrary.wiley.com/doi/pdf/10.1002/jrs.4335, URL https://analyticalsciencejournals.onlinelibrary.wiley.com/doi/abs/10.1002/jrs.4335.

[43] T.C. Strekas, T.G. Spiro, Cytochrome c: Resonance Raman spectra, Biochimica Biophys. Acta (BBA) - Protein Struct.re 278 (1) (1972) 188–192, http://dx.doi.org/10.1016/0005-2795(72)90121-3, URL https://www.sciencedirect.com/science/article/pii/0005279572901213.

[44] S.G. Kruglik, B.-K. Yoo, J.-C. Lambry, J.-L. Martin, M. Negrerie, Structural changes and picosecond to second dynamics of cytochrome c in interaction with nitric oxide in ferrous and ferric redox states, Phys. Chem. Chem. Phys. 19 (2017) 21317–21334, http://dx.doi.org/10.1039/C7CP02634J.

[45] H.-J. van Manen, N. Uzunbajakava, R. van Bruggen, D. Roos, C. Otto, Resonance Raman imaging of the NADPH oxidase subunit cytochrome b558 in single neutrophilic granulocytes, J. Am. Chem. Soc. 125 (40) (2003) 12112–12113, http://dx.doi.org/10.1021/ja036973r, PMID: 14518995.

[46] Y.E. Nikiforov, R.R. Seethala, G. Tallini, Z.W. Baloch, F. Basolo, L.D.R. Thompson, J.A. Barletta, B.M. Wenig, A. Al Ghuzlan, K. Kakudo, T.J. Giordano, V.A. Alves, E. Khanafshar, S.L. Asa, A.K. El-Naggar, W.E. Gooding, S.P. Hodak, R.V. Lloyd, G. Maytal, O. Mete, M.N. Nikiforova, V. Nosé, M. Papotti, D.N. Poller, P.M. Sadow, A.S. Tischler, R.M. Tuttle, K.B. Wall, V.A. LiVolsi, G.W. Randolph, R.A. Ghossein, Nomenclature revision for encapsulated follicular variant of papillary thyroid carcinoma: A paradigm shift to reduce overtreatment of indolent tumors, JAMA Oncol. 2 (8) (2016) 1023–1029, http://dx.doi.org/10.1001/jamaoncol.2016.0386, arXiv:https://jamanetwork.com/journals/jamaoncology/articlepdf/2513250/coi160009.pdf.

[47] P.W. Rosario, G.F. Mourão, Noninvasive follicular thyroid neoplasm with papillary-like nuclear features (NIFTP): A review for clinicians, Endocrine-Related Cancer 26 (5) (2019) R259 – R266, http://dx.doi.org/10.1530/ERC-19-0048, URL https://erc.bioscientifica.com/view/journals/erc/26/5/ERC-19-0048.xml.

[48] C.C. Juhlin, O. Mete, Z.W. Baloch, The 2022 WHO classification of thyroid tumors: Novel concepts in nomenclature and grading, Endocrine-Related Cancer 30 (2) (2023) e220293, http://dx.doi.org/10.1530/ERC-22-0293, URL https://erc.bioscientifica.com/view/journals/erc/30/2/ERC-22-0293.xml.

[49] B.R. Haugen, A.M. Sawka, E.K. Alexander, K.C. Bible, P. Caturegli, G.M. Doherty, S.J. Mandel, J.C. Morris, A. Nassar, F. Pacini, M. Schlumberger, K. Schuff, S.I. Sherman, H. Somerset, J.A. Sosa, D.L. Steward, L. Wartofsky, M.D. Williams, American Thyroid Association Guidelines on the management of thyroid nodules and differentiated thyroid cancer task force review and recommendation on the proposed renaming of encapsulated follicular variant papillary thyroid carcinoma without invasion to noninvasive follicular thyroid neoplasm with papillary-like nuclear features, Thyroid® 27 (4) (2017) 481–483, http://dx.doi.org/10.1089/thy.2016.0628, PMID: 28114862.

[50] J. Surmacki, B. Brozek-Pluska, R. Kordek, H. Abramczyk, The lipid-reactive oxygen species phenotype of breast cancer. Raman spectroscopy and mapping, PCA and PLSDA for invasive ductal carcinoma and invasive lobular carcinoma. Molecular tumorigenic mechanisms beyond warburg effect, Analyst 140 (2015) 2121–2133, http://dx.doi.org/10.1039/C4AN01876A.

[51] I. Kholová, D. Kalfert, J. Lintusaari, E. Rajakorpi, M. Ludvíková, Follicular epithelial dysplasia as Hashimoto thyroiditis-related atypia: A series of 91 specimens, Endocrine Pathol. 32 (3) (2021) 368–374.